Class. Quantum Grav. **16** (1999) 1487–1502. Printed in the UK PII: S0264-9381(99)98791-9

Doppler measurement of the solar gravitational deflection

Luciano Iess†, Giacomo Giampieri‡, John D Anderson§ and Bruno Bertotti‖

† Dipartimento Aerospaziale, Università di Roma 'La Sapienza', 00184 Rome, Italy
‡ Astronomy Unit, Queen Mary and Westfield College, London E1 4NS, UK
§ Jet Propulsion Laboratory, California Institute of Technology, Pasadena, CA 91109, USA
‖ Dipartimento di Fisica Nucleare e Teorica, Università di Pavia, 27100 Pavia, Italy

Received 28 October 1998

Abstract. Testing alternative metric theories of gravity with an accuracy much better than the present level has recently drawn great attention, in particular in relation to the search for a very weak scalar field, a possible remnant of an early inflationary cosmology. The gravitational deflection of electromagnetic waves is controlled by the dimensionless post-Newtonian parameter γ, which takes a value of unity in general relativity. In this work we claim that the accuracy in the measurement of γ can be substantially improved by measuring the Doppler frequency shift of a microwave beam transponded back to the ground by an interplanetary spacecraft near solar conjunction. In this kind of experiment, the dispersion due to the plasma in the solar corona is the crucial difficulty, which, however, can be essentially overcome using skilful combinations of carriers with different frequencies. The spacecraft Cassini, launched in 1997, adopts a sophisticated radio system, including a Ka-band link at 32–34 GHz, which makes this possible. We discuss the noise budget for two experiments to be carried out with Cassini in 2002 and 2003. In particular, we consider the contribution of the solar corona, the non-gravitational accelerations, and thermal noise due to solar radio emission. We estimate that an accuracy in γ of about 10^{-5} is achievable.

PACS numbers: 0480C, 0450, 9555S, 9660P, 8440V

1. Introduction

Metric theories of gravity, including general relativity, predict that photons passing near the Sun are deflected by an angle

$$\theta_{gr}(b) = \frac{2(1+\gamma)GM_\odot}{b\,c^2} \simeq 8\times 10^{-6}\left(\frac{1+\gamma}{2}\right)\left(\frac{R_\odot}{b}\right), \tag{1}$$

where b is the impact parameter of the ray, $GM_\odot/c^2 = 1.48$ km is the gravitational radius of the Sun and $R_\odot$ is its radius. The bending effect is thus controlled by the parameter γ, whose value is unity in general relativity. Its present empirical value is [1]

$$\gamma = 1.000 \pm 0.001, \tag{2}$$

where the quoted uncertainty is a rough estimate of the results of different measurements.

The parametrization of the gravitational deflection with the dimensionless parameter γ belongs to the 'parametrized post-Newtonian' (PPN) formalism, with which a wide class of metric theories of gravitation and their experimental consequences are described in a multi-dimensional parameter space. In the simplest case this space has two dimensions, γ and β, with general relativity at (1, 1). Different experiments are governed by different combinations of these two parameters: for example, for the secular advance of the periastron we have

0264-9381/99/051487+16$19.50

$(2-\beta+3\gamma)/3$; for the violation of the principle of equivalence the combination is $4\beta-3-\gamma$ [2], which occurs in lunar theory if the contributions of the internal binding energy of the Earth to the inertial and gravitational masses are different. From the lunar laser ranging data the last parameter is constrained to be less than 10^{-3}, providing a measurement of β more precise than that obtainable from the Mercury perihelion test.

After the 80 years since general relativity was born, Einstein's theory has, so far, survived every test. This rare and remarkable longevity, along with the absence of any adjustable parameters, motivates more accurate tests and invites the question, at what level of accuracy is it violated? As a result of tests performed so far, most alternative theories have been put aside; only those theories of gravity flexible enough to accommodate the experimental constraints have survived, a protection provided by additional free parameters and coupling constants. The Brans–Dicke [3] theory is conceptually one of the most attractive competitors to general relativity. It contains, besides the metric tensor, a scalar field ϕ and an arbitrary coupling constant ω, which is related to the parameter γ by

$$\gamma = \frac{1+\omega}{2+\omega}. \tag{3}$$

The present limit (2) on γ gives the constraint $|\omega| > 500$. In addition, many scalar–tensor (ST) theories have been proposed, generalizing the original Brans–Dicke concept. In all such theories the coupling function depends on the value of the scalar field, $\omega = \omega(\phi)$, and therefore changes in time with the evolution of the universe. Because of recent developments in cosmology (e.g. inflationary models) and elementary-particle physics (e.g. string theory and Kaluza–Klein theories), these ST theories are considered the most interesting alternatives to general relativity. As pointed out by various authors (see [4, 5] and references therein), a large class of ST theories contain an attractor mechanism toward general relativity in a cosmological sense. If this is how the universe is actually evolving, then today we can expect, from equation (3), a very small discrepancy of the order of

$$|\gamma - 1| \approx 10^{-7}\text{–}10^{-5}, \tag{4}$$

where the exact value depends on the particular ST theory adopted for the cosmological calculations [5]. This kind of argument provides a strong motivation for experiments able to push beyond the present empirical accuracy on γ.

Apart from traditional observations during solar eclipses (see, e.g., [6]), the bending effect has, so far, been tested with two methods. The measurement of the deflection itself is best performed differentially with two (natural or artificial) radio sources close to the Sun on the celestial sphere. Thanks to advanced very long baseline interferometric (VLBI) techniques it is now possible to achieve accuracies in angular measurements of the order of hundreds of microarcsec [7]. A series of recent observations yielded a value $\gamma = 1.000 \pm 0.002$ [8], comparable in accuracy with that quoted in equation (2). Recently, Lebach *et al* [9] and Eubanks *et al* [10] have announced a new accurate VLBI determination, based on a large database of more sensitive observations, claiming an accuracy of 6×10^{-4}.

Secondly, the solar gravity induces an increase in the light travel time (the 'range') to a planet or spacecraft near solar conjunction. This effect in radar propagation was first pointed out by Shapiro [11]. In the isotropic form of the solar metric, the one-way light time t from the Earth to a spacecraft, respectively, at a distance ℓ_0 and ℓ_1 from the Sun, suffers a relativistic correction

$$\Delta t = (1+\gamma)\frac{GM_\odot}{c^3}\ln\left(\frac{\ell_0+\ell_1+t}{\ell_0+\ell_1-t}\right) \approx (1+\gamma)\frac{GM_\odot}{c^3}\ln\left(\frac{4\ell_0\ell_1}{b^2}\right). \tag{5}$$

The separation of this correction from the much larger Newtonian light-time is made possible by the characteristic logarithmic dependence of the relativistic effect on the impact parameter

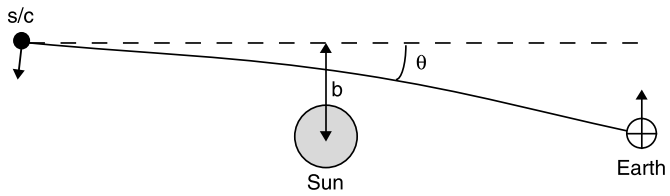

Figure 1. The geometry of the effect.

b and hence on the time of observation. The determination of γ quoted in equation (2) has been obtained with the Viking landers, anchored to the surface of Mars [12], while the more recent free-flying Voyager 2 test yielded a standard error for γ of 0.03 [13], comparable to previous Mariner tests performed 25 years ago [14].

As pointed out by Shapiro in 1964 [15], since the delay correction changes with time, there must also be a correction in the relative velocity along the line of sight, hence a Doppler effect. One can find its order of magnitude by noting that the deflection changes the component of the velocity of the photon along the trajectory of the two end points by an amount $\approx v\theta_{gr}$ (figure 1); since $v = 10^{-4}c$ the effect is of order

$$\frac{v}{c}\theta_{gr} \approx 8 \times 10^{-10}\left(\frac{R_\odot}{b}\right). \tag{6}$$

We have thereby a third way of measuring γ [16].

Although it is possible to measure the time delay by integrating the measured Doppler shift, we stress that the Doppler technique is quite different from the ranging method. The latter is currently used in interplanetary navigation and is especially useful when absolute measurements of distance are required. It uses a wide-band microwave signal with a periodic phase modulation transmitted to the spacecraft and transponded back to the ground. The correlation between the incoming signal and a Doppler-shifted replica stored at the ground antenna is measured with a variable delay; the delay at which the correlation is largest is the round-trip light time [12, 14]. Accuracies of a few metres are currently achieved far from the solar corona. In Doppler measurements one uses as an observable quantity the frequency of a very stable, coherent microwave signal, which provides the relative velocity averaged over a suitable integration time τ [17]; the specification for its accuracy in the CASSINI mission (Ka band) is 10^{-4} cm s^{-1} for integration times up to 10 000 s. Thus, one measures the *change* in the distance over this time with the far better accuracy of 3 cm (see equation (7) below). The time scale of the relativistic experiment is, however, larger than 10 000 s and depends upon the impact parameter; if, after the proper processing, the final spectrum of the frequency fluctuations turns out to be red, then we can expect some deterioration.

This paper is organized as follows. In section 2 we introduce the Doppler observable, and describe its gravitational component. In section 3 we describe the Cassini experiments. Section 4 considers the effect of the solar corona plasma. The performances of the radio links when tracking near the Sun are discussed in section 5, with emphasis on system temperature increase and diffraction effects; finally, in section 6 we analyse the effect of non-gravitational forces.

2. The measurement

Experiments based on range-rate observables were studied informally more than 20 years ago by one of us (JDA), but they were abandoned because of the limitations of the S-band radio systems at that time. At those frequencies (2.1–2.3 GHz), in fact, the phase scintillation due to the solar corona is so large that the relativistic Doppler shift cannot be measured at an interesting level. The Cassini mission, launched in October 1997 and due to explore the Saturnian system, is equipped with a sophisticated radio system, capable of handling at the same time carriers in X and Ka bands (7.9–8.4 and 32–34 GHz, respectively), thus drastically reducing the coronal plasma noise.

In order to achieve the highest accuracy, the Doppler frequency shift of the carrier wave is referenced to ground-based atomic frequency standards. The observable is the fractional frequency shift of a stable and coherent two-way radio signal (Earth–spacecraft–Earth)

$$y(t) = \frac{\nu_R(t) - \nu_T}{\nu_T} = \frac{2}{c}\frac{\mathrm{d}L}{\mathrm{d}t}, \tag{7}$$

where ν_R and ν_T are, respectively, the transmitted and received frequencies, t is the receiving time and $2L$ is the overall optical distance (including diffraction effects) traversed by the photon in both directions. This technique has various applications, from the estimate of the gravity field of planetary systems (see [18–20] for recent examples), to the study of interplanetary plasma [21, 22], and the attempts to detect low-frequency gravitational waves [23–26]. Interplanetary Doppler tracking near solar conjunction, as a tool for testing relativistic effects, has been discussed previously in [16, 27].

The expected relativistic contribution to the Doppler shift is given by [16, 27]

$$y_{gr}(t) = \frac{2}{c}\left(\frac{v_1\ell_0 + v_0\ell_1}{\ell_0 + \ell_1}\right)\theta_{gr}(b) = 4(1+\gamma)\frac{G\,M_\odot}{b\,c^3}\frac{\mathrm{d}b}{\mathrm{d}t}, \tag{8}$$

where v_0, v_1 are, respectively, the transverse velocities of the Earth and the spacecraft, and ℓ_0, ℓ_1 are their distances from the Sun. The time scale is $b/\dot{b} \approx b/v(b/R_\odot) = 7 \times 10^4$ s for $b = 2R_\odot$. Note that the effect depends on time essentially through the impact parameter b. The last equality in equation (8) is obtained by inserting equation (5) into equation (7).

Equation (8) relates the gravitational Doppler shift to the more familiar expressions for the angular deflection and time delay. As mentioned in the introduction, the deflection of light rays, the time delay of radio signals and the frequency shift are different manifestations of the same aspects of the solar gravitational field. Indeed, it is equally possible to obtain the frequency shift by integrating the equations of motion of photons in the solar metric and derive the time delay and the angular deflection from the Doppler shift. Of course, measuring the three effects involves completely different experimental techniques.

For the geometry of the Cassini conjunction in June 2003, the maximum gravitational Doppler shift is 7.5×10^{-10} (see figure 2). This signal can be compared with the expected measurement noise in y (characterized by its Allan deviation†). For advanced planetary missions such as Cassini, equipped with multi-frequency links at the X and Ka bands, Allan deviations $\sigma_y \simeq 10^{-14}$ for averaging times between 1000 and 10 000 s are achievable even near solar conjunctions [28]. This corresponds to a maximum signal-to-noise ratio of 7.3×10^4 and an accuracy in the measurement of γ of 1.3×10^{-5}. Although this estimate is a very rough one, it is apparent that a significant improvement is to be expected; note also that the time dependence of the delay is known exactly, which will increase the accuracy in γ after the

† The Allan deviation is the most used figure of merit for the characterization of frequency stability of oscillators. It is defined as $\sigma_y(\tau) = [0.5\langle(\bar{y}_{i+1}(\tau) - \bar{y}_i(\tau))^2\rangle]^{1/2}$ where $\bar{y}_i(\tau) = \frac{1}{\tau}\int_{t_i}^{t_i+\tau} y(t)\,\mathrm{d}t$.

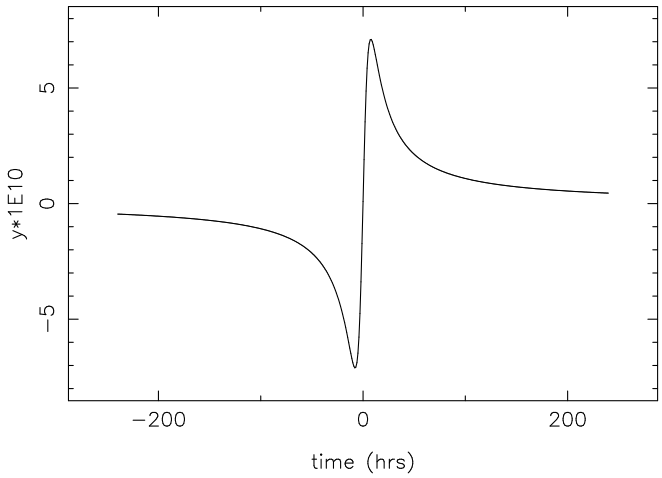

Figure 2. The relativistic contribution to the observable $y = (2/c)\,\mathrm{d}L/\mathrm{d}t$ for the Cassini solar conjunction in June–July 2003.

fit. The main purpose of this paper is to quantify this expectation, through a discussion of the main noise sources.

3. The Cassini experiment

The sophisticated radio system of the Cassini mission exploits a multi-frequency link in the X and Ka bands to ensure the highest frequency stability. Transponders on board allow a stable lock of the transmitted to the received phase. An additional Ka-band downlink is locked to the X phase on board, thus providing three different observables. These unique capabilities of the radio system require adequate support from the ground segment. The Deep Space Network (DSN) is building, for this purpose, a new experimental station at the Goldstone complex in California (DSS 25), with stringent requirements and new technology. DSS 25 is a beam waveguide antenna especially built to support Cassini radio science experiments. In its full configuration, the radio link will include two simultaneous, two-way, coherent Doppler links at X (7175 MHz uplink, 8425 MHz downlink) and Ka (34 316 MHz uplink, 32 028 MHz downlink) and a third, mixed link in which a Ka-band downlink carrier is coherent with the X-band uplink (figure 3). Less complex configurations are also possible.

The performance of the Ka link is expected to be better than the standard X-band configuration. Its overall phase stability, measured by the Allan deviation, is required to be $\sigma_K \leqslant 3 \times 10^{-15}$ at integration times between 1000 and 10 000 s. At X band the specification is roughly a factor of three larger. Achieving such an outstanding stability requires not only a careful electronic and mechanical design of the antennas, but also a large effort to provide good calibration for media effects, especially tropospheric water vapour. To this end, a new generation of water vapour radiometers is under development. Unfortunately, the new station at Goldstone will be able to track Cassini only for about one-third of the observing time. In Italy, a new 64 m high-frequency antenna, to be used for radioastronomy and deep-space communications, has been recently funded. Its capabilities include reception, and hopefully transmission, also in the Ka band. Due to the excellent visibility of Cassini from the northern hemisphere during the 2002 and 2003 solar conjunctions, the Goldstone antenna and the

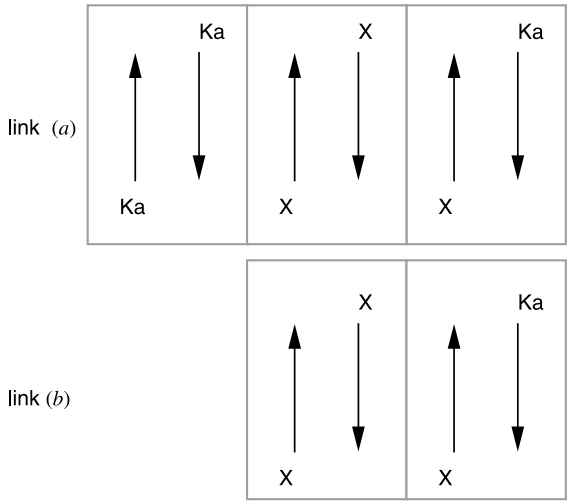

Figure 3. The combinations of coherent links to be considered. (*a*) X and Ka up and down, with an additional Ka down-locked to the X phase on board (three observables). (*b*). X up and down, Ka down locked to the X phase on board (two observables). Combination (*a*) is the prime operation mode of the experiment, but will be available for only $\frac{1}{3}$ of the time, or for more than $\frac{2}{3}$ of the time if the Sardinia antenna will be available. Combination (*b*) is a backup.

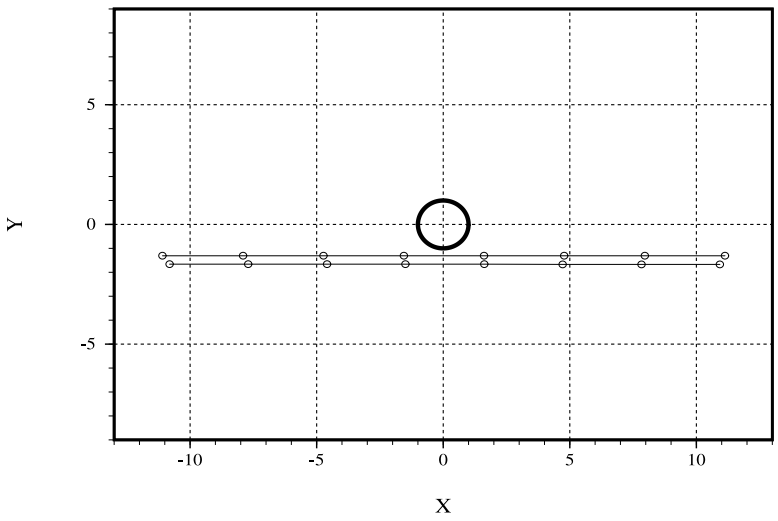

Figure 4. The trajectory of Cassini projected in the plane passing through the Sun and normal to the Earth–Sun direction, as seen from an observer on the Earth, during the conjunction experiments of 2002 (top) and 2003 (bottom). The ticks are separated by 1 day.

new one in Italy would provide up to 20 h of daily coverage, with great benefits for the experiment.

During cruise, in two periods lasting 30 days around two solar conjunctions occurring on June 21, 2002 and July 1, 2003, Cassini will be continuously Doppler tracked to measure the gravitational deflection with unprecedented accuracy. Figure 4 shows the trajectory of

the spacecraft projected on the plane through the Sun normal to the Sun–Earth direction. The geometries of the two conjunctions are almost ideal, thanks to the fact that the minimum impact parameter is only a little larger than $R_\odot$, so that we obtain the strongest possible signal, without missing any data because of occultation. In fact, small values of b are important; this is an important difference with the delay experiment, where the observable depends logarithmically on b. We also note that the special relativistic Doppler effect, not considered here, has its minimum near conjunction, where the velocities are almost orthogonal to the photon's path and the second-order Doppler shift dominates.

Of course, the subtraction of this contribution, as well of the much larger contribution of the ordinary (i.e. non-relativistic) Doppler effect, must be done with a very accurate knowledge of the orbit. To see how accurately, note that the relativistic effect corresponds to a (variable) acceleration of order $v^2\theta_{gr}/b = 3 \times 10^{-3}$ cm s^{-2}; therefore the relative acceleration of the spacecraft and the station must be known to, say, 10^{-8} cm s^{-2}, while the acceleration of the Earth around the Sun is 0.6 cm s^{-2}. The ordinary Doppler effect results mainly from this interplanetary motion, which can be measured accurately during the cruise, and the term due to the rotation, which requires a good knowledge of the polar motion and the position of the station.

4. Coronal and interplanetary plasma effects

In a radio experiment near solar conjunction, the coronal plasma is the main source of noise. Were the spacecraft equipped with a hydrogen maser, so that the uplink and the downlink frequency shifts could be measured separately, the differential Doppler technique (see [16]) could reduce the plasma contribution by at least three orders of magnitude. A similar technique was used by Vessot and Levine [29] in a redshift experiment. For Cassini, which does not have a hydrogen maser, multi-frequency radio links will be used instead [28, 30].

If no plasma compensation is possible, as in the case of a single-frequency radio link, the noise can be so large as to hide the relativistic effect. Thanks to the fact that the plasma effect is dispersive, in past interplanetary missions a partial plasma compensation was made possible by dual-frequency transmission from spacecraft to ground, usually at S (2.3 GHz) and X (8.4 GHz) bands. The Viking experiment exploited this capability of the orbiter to significantly reduce the plasma noise, which, however, remained the largest error source. The dual-frequency downlink allows a nearly complete plasma calibration of the returning signal, while the uplink contribution can only be estimated in a statistical way. This configuration of the ground and flight hardware remained essentially unmodified for nearly 20 years, which incidentally explains why no other space experiment could hope to improve the accuracy of the Viking results. This limitation of interplanetary radio links will be overcame with new advanced tracking stations.

As a side product of the relativity experiment, Cassini's Doppler data can thus provide valuable information about the solar and interplanetary plasma. This method, along with its limitations, has been fully investigated in [30]. In particular, it can be shown that with the full link, as shown in figure 3(*a*), one can measure the whole plasma columnar content in the electric approximation, being limited only by the effect of the magnetic field and by refraction. Alternatively, one can focus on the solar corona only, thus accessing minor corrections to the electric approximation.

Before the introduction in deep-space communications of multi-frequency tracking and Ka-band signals, measuring γ using the Doppler observable was not competitive with the ranging technique, where small impact parameters are not needed to obtain large signals. Moreover, at the lower frequencies used so far, the solar corona posed insuperable difficulties,

not only because of the much larger plasma noise, but also, at a more fundamental level, due to the impossibility of tracking the carrier.

The fundamental limit of plasma calibrations based on multi-frequency links stems from the residual lack of coherence between the links at different frequencies [28]. This is essentially due to thermal and other noises on the ground and onboard electronics (transmitters and receivers). The plasma calibration is affected by an error determined by the transponding ratios and thermal noise in each chain. For Cassini, the leading contribution to this error comes from the phase instability of the Ka-band link, which is, however, a factor of three smaller than the instrumental noise in the other links. If we attribute to the electronics all the expected, residual phase noise at the Ka band (3×10^{-15} for time scales between 1000 and 10 000 s), the estimate provided in [28] yields a value 7×10^{-15} for the error in y. As will be discussed in the next section, the increased system noise due to the presence of the Sun in the antenna beam suggests a more conservative estimate. In the following we will use the value $\sigma_y \simeq 10^{-14}$.

Our preliminary analysis shows that the prospects for an almost complete cancellation of the coronal plasma with the optimal configuration (figure 3(*a*)) are very good. When the Ka-band uplink will not be available, a partial compensation for the plasma is still possible using the backup link combination (shown in figure 3(*b*)), more satisfactory than a single X-band link [30]. With this scheme the uplink phase in the X band onboard is locked to both the X and Ka downlinks. The difference $y_X - y_K$ between the corresponding fractional frequency changes, therefore, depends only upon the dispersive part of the downlink path, and can be used to determine its columnar electron content. In general, at least for frequencies which are not much smaller than the reciprocal of the round-trip light time $2L/c$, this content is different from the corresponding uplink contribution. However, if it is concentrated near the point of the beam nearest to the Sun, one can use its measurement to subtract the plasma contribution from the uplink photons which pass at that point at the same time. This method becomes less efficient as the impact parameter grows much larger than the solar radius; also, it has never been really tested in actual data.

It is interesting to note that, since plasma effects near the Sun need to be eliminated to better than one part in 10^4, the usual expression for the frequency correction (7) (where L is the optical path with suitable refractive index) is not accurate enough. Relativistic corrections $O(v/c)$ are needed, in particular the one arising from the difference between the emission and the receiving time. The fully relativistic expression of the Doppler effect in a moving medium has been derived with the Hamiltonian formalism in [31].

5. Solar effects on carrier tracking

Tracking a spacecraft near the Sun involves a substantial increase in the system temperature and a degradation of the signal-to-noise ratio (SNR). The main concern is the possible failure of ground and onboard receivers to detect the carrier's signal and to track its phase correctly. As a consequence of the decrease in SNR, one may also expect a lower stability of the radio link and therefore a poorer ability to calibrate plasma noise. We will show that both effects are negligible.

A potentially more dangerous effect is due to amplitude scintillation of the signal as it propagates through the solar corona. Each coronal inhomogeneity acts as a scattering centre for the impinging electromagnetic wave. At the receiver the electric fields of the scattered waves add up, producing a time-varying interference pattern that may lead to large amplitude fluctuations. The dimension of spatial inhomogeneities giving rise to diffraction at a distance D from the corona depends on the radio wavelength λ and is of the order of the Fresnel zone $(\lambda D)^{1/2}$ (about 100 km for Ka band at 7 AU). Amplitude scintillation (also called interplanetary

scintillation or IPS) has been observed for spacecraft and natural radio sources and is an important tool to probe the solar corona at small scales [32]. Two quantities are relevant to the experiment proposed here: the magnitude of intensity fluctuations, measured by the scintillation index $m =$ (RMS intensity fluctuations about the mean)/(mean intensity), and the time scales of such variations.

Measurements of m at different wavelengths [32, 33] have shown that the strong-scintillation regime ($m \approx 1$) is reached in X band at approximately $6R_\odot$. The index m has a strong dependence on frequency, being roughly proportional to ν^{-p} with $p \approx 2.5$. In normal coronal conditions, the Ka band signal will never exhibit strong scintillation. At X band one therefore expects strong fluctuations of the signal level (of 20 dB or more), for time scales varying from milliseconds to seconds. The statistical characterization of these extreme events is largely unknown, essentially due to lack of observations. In general, the onboard X-band transponder might lose the uplink carrier when tracking near the Sun in the presence of extraordinary coronal activity. On the other hand, the large SNR provides a good safety margin against most of these events (see later). This problem is even less critical in the downlink, because the signal is tracked using broadband digital receivers. Successful two-way tracking of spacecraft has already been performed in the past at S band below $2R_\odot$ [34, 35], close to solar minimum.

Two other physical optics effects come into play: spectral broadening and angular broadening. The latter is due to the fact that the coronal fluctuations effectively broaden the size of a radio source, which appears to have finite angular dimension. If the angular broadening is larger than the beam width of the receiving antenna, a degradation of SNR occurs. By using the results of [35] one may show, however, that at X band this effect, which roughly scales as λ^2, is always negligible, even for ground antennas, whose beamwidth is much narrower.

Spectral broadening of a monochromatic carrier originates from temporal fluctuations of the received phases due to the motion of the scattering centres in the solar corona. Below $2R_\odot$ spectral broadenings up to 200 Hz have been observed at S-band frequencies [35]. For an X-band signal this figure, being proportional to λ^2, is reduced by a factor of 10 and therefore is well within the typical bandwidths of deep-space transponders (for Cassini about 180 Hz at the expected signal levels). The SNR levels over the receiver bandwidth are therefore substantially unaffected.

The emission from the Sun at microwave frequencies depends, in general, on the phase of the solar cycle. The effect is larger at solar maximum and smaller at solar minimum. For most of the time the emitted flux is almost steady over short time scales, but occasionally, during periods of large activity, it may increase by up to a factor of ten over time scales from a few minutes to several hours, depending on the type of radio burst. If these emissions occur during the experiment, the radio link may be seriously impaired. However, the probability of occurrence of such extraordinary events during the experiment is small, and we will consider here only the steady emission from the quiet Sun.

The solar luminosity in a bandwidth B at the wavelengths of the radio carriers can be computed using the Jeans approximation. The flux emitted by a surface element $\mathrm{d}S$, in a unit time, solid angle $\mathrm{d}\Omega$ and bandwidth $\mathrm{d}\nu$ about the frequency $\nu = c/\lambda$ is

$$\mathrm{d}P = \frac{2kT_\odot}{\lambda^2}\,\mathrm{d}S\,\mathrm{d}\nu\,\mathrm{d}\Omega. \tag{9}$$

To obtain the total power emitted from the Sun, one needs to integrate $\mathrm{d}P\cos\theta$ over the external half-space and the surface of the Sun

$$P_s = \frac{2kT_\odot B}{\lambda^2} 4\pi^2 R_\odot^2. \tag{10}$$

Here $T_\odot$ is the effective temperature of the Sun. At centimetric wavelengths, $T_\odot$ varies between 10^4 and 10^5 K [36]. A reference value of 2×10^4 K at X band and 1×10^4 K at Ka band will be assumed in the following calculations. The actual effective temperature may be larger by up to a factor of four in periods of large solar activity. The power (10) corresponds to a flux of about 2.5×10^{-20} and 2.5×10^{-19} W m^{-2} Hz^{-1}, respectively, at 7.2 and 32.0 GHz, at the Earth's distance.

The spacecraft and ground-based antennas are both affected by the solar noise, which causes an increase in the system noise temperature and a decrease in SNR, depending on the proximity of the beam to the Sun. The total SNR, the ratio between the carrier's power and the noise power, is the sum of the contributions from the uplink (u) and the downlink (d) (see, for example, [37]):

$$\mathrm{SNR} = (\mathrm{SNR}_u^{-1} + \mathrm{SNR}_d^{-1})^{-1}. \tag{11}$$

In each link, denoted by the index i, the SNR is given by

$$\mathrm{SNR}_i = \frac{C_i}{N_i} = \frac{\eta_i}{L_{is} L_a} \frac{G_{it} G_{ir}}{k T_i B_i + N_{is}}, \tag{12}$$

where C represents received carrier power, N represents total noise power, η represents effective isotropic radiated power, $L_s = (4\pi L/\lambda)^2$ represents space loss for a wavelength λ and distance L, L_a represents atmospheric and antenna losses, $G_{t,r}$ represents receiving and transmitting antenna gain, T represents effective noise temperature (without contribution from the Sun), k represents the Boltzmann constant, B represents receiver bandwidth and N_s represents the noise power due to the Sun.

The parameters relevant to the Cassini radio link are summarized in table 1. When no hot body is in the beam, equation (12) leads to a link budget dominated by the downlink contribution (see table 2).

Table 1. The Cassini radio link parameters. The spacecraft antenna gain in the Ka-band uplink was degraded by design in order to match the performances of the attitude control system. The onboard transmitter power at Ka band refers to each of the two carriers.

	Spacecraft	Ground
Antenna diameter (m)	4	34
Half-power beamwidth (deg)	0.65° (X up), 0.57° (X down)	0.074° (X up), 0.063° (X down)
	0.17° (Ka up), 0.17° (Ka down)	0.016° (Ka up), 0.016° (Ka down)
Antenna gain (dBi)	45.4 (X up), 47.2 (X down)	66.9 (X up), 68.0 (X down)
	55.7 (Ka up), 56.4 (Ka down)	78.4 (Ka up), 77.2 (Ka down)
Transmitter power (W)	19 (X)	4000 (EIRP = 132.8 dBm) (X)
	2.7 (Ka)	800 (EIRP = 137.3 dBm) (Ka)
Receiver noise temperature (K)	275 (X), 750 (Ka)	25(X), 80 (Ka)

Table 2. Link budget for the conjunction experiment in June 2003 ($L = 9.4$ AU), with no hot-body contribution. C is the received power, $\tilde{N}$ the noise power per unit bandwidth. The quantity 1/SNR per unit bandwidth is $\tilde{N}/C$. Atmospheric, polarization and antenna losses are included. The actual SNR figures may be smaller by up to 2 dB, due to pointing errors.

	X up	X dn	Ka up	Ka dn (1)	Ka dn (2)
C (dBm)	−116.8	−137.3	−116.2	−135.3	−139.2
$\tilde{N}$ (dBm Hz)	−174.2	−184.7	−169.9	−179.6	−179.6
$C/\tilde{N}$ (dB)	57.4	47.4	53.7	44.3	40.4

When the Sun is close to the beam, the SNR is degraded by an amount which depends on the design characteristics of the antenna. A precise calculation would require the integration of the radio emission from each portion of the solar disc over the antenna pattern. For the ground station, which has a beamwidth much smaller than the angular diameter of the Sun, an assessment of this contribution may be obtained from existing measurements for the DSN 34 m network, at X band. The antenna pattern far from the main lobe is such that the actual solar noise temperature may be approximated by the following expression [34]:

$$T_s = 800 \exp(-\delta/0.5^\circ) \text{ K}, \tag{13}$$

where δ is the angle between the Sun and the axis of the antenna (solar aspect angle). The coefficient 800 is an average value: in practice the solar radio flux can vary by as much as a factor of two. During the 2003 Cassini experiments, δ reaches the minimum value 0.35°. This yields a value of 400 K as the maximum increase in the antenna temperature, corresponding to a noise power of -172.6 dBm Hz and a SNR degradation of 12.1 dB with respect to normal operating conditions. The solar noise equals the noise power shown in table 2 (which does not include hot-body contributions) at a solar aspect angle of 1.7°, when the impact parameter is about $7R_\odot$. As there is enough carrier margin even at the closest approach, the capability of tracking the spacecraft is not impaired. Measurements performed at Ka band with a 34 m dish (DSS-13) have shown a much smaller increase in the noise temperature, at a level of about 200 K at 0.35° from the Sun [38]. One may conclude that the risk of losing the carrier from the ground station is negligible, even at the minimum impact parameter. In any case, broadband recording of the signal by means of open-loop receivers would allow the recovery of the signal.

In spite of the larger SNR, one might expect in principle a less favourable situation in the uplink, because the half-power beamwidth is comparable to the angular diameter of the Sun (0.57°). An evaluation of the solar radio noise on the spacecraft may be obtained by assuming that all the power is emitted by a point source (e.g. the centre of the Sun) at an angular distance δ from the optical axis of the onboard antenna (see also equation (12)):

$$N_s = \frac{P_s}{L_s} G_{sc}(\delta). \tag{14}$$

Here G_{sc} is the gain of the spacecraft antenna as a function of the solar aspect angle and P_s is defined in equation (10). Using equation (10) and considering the extreme case $\delta = 0$, one obtains an upper limit to the solar noise power of -203.1 and -169.2 dBm Hz, respectively, at X (7.2 GHz) and Ka band (32.0 GHz) for the solar conjunction of 2002, occurring at a heliocentric range of 7.4 AU. At X band the hot-body noise is therefore at least 29.8 dB below the noise power of the onboard receiver. At Ka band, where the effect is more severe, one would obtain a maximum increase of the system noise of just 3 dB. Even in this unrealizable and extreme situation, onboard transponders could reliably track the carrier.

The increased noise power degrades the frequency stability of the radio link. This effect influences mostly the ground station, as the system noise power onboard the spacecraft increases only by a negligible amount. For pure white phase noise, the contribution of the receiver to the total Allan deviation is inversely proportional to the square root of the SNR. The receiver Allan deviation at 1000 s may therefore rise up to 2.4×10^{-15}, a value almost equal to the expected stability of the link (3×10^{-15}). According to the results of [28] this would lead to a decrease (by about 30%) in the accuracy of the plasma noise compensation.

As a conclusion to this discussion on the solar effects, it is apparent that the spacecraft tracking at X band below $2R_\odot$ is affected by several uncertainties, mostly dependent on the level of solar activity. The occurrence of both conjunctions close to the solar maximum is a reason for concern. No difficulty should be expected in the Ka-band link. In quiet coronal conditions the SNR level is sufficiently large to ensure good immunity to amplitude fluctuations

and increased radio emission from the Sun, the spectral broadening has a limited effect and the ability to perform plasma compensation at the 10^{-15} level is not impaired.

6. Non-gravitational accelerations

Unmodelled, non-gravitational accelerations are a potential source of systematic errors in the measurement. The problem is more severe in those cases where the gravitational signal changes slowly with time, as in tests based on time delay. Indeed, the excellent accuracy of the Viking experiment was largely due to the use of the Mars lander (virtually immune to the effect of non-gravitational accelerations) as the end point of the radio link. In this section we will evaluate the perturbing forces for Doppler experiments, and show that their contribution to the measurement error is negligible.

We will consider five sources of non-gravitational accelerations: (1) solar radiation, (2) solar wind pressure, (3) emitted radio power, (4) anisotropic thermal radiation of the spacecraft and (5) attitude motions. Although one could, in principle, set up complicated engineering models to predict at least some of these effects, it may turn out that their final accuracy does not meet completely the tight requirement of this experiment, in spite of the significant effort required. A better approach is to accept our ignorance about non-gravitational accelerations and assess to what extent they can be assumed constant over the time scale of the relativistic effect. In fact, a constant acceleration produces a linear frequency drift that can be accounted for in the data analysis by a single unknown parameter. The short duration of the experiment makes this strategy even more meaningful. This remark is particularly relevant also in relation to the recent claim of a constant acceleration, of unknown origin, of about 8×10^{-8} cm s^{-2} acting upon some interplanetary spacecraft [39].

The figure against which we compare the effects of the non-gravitational accelerations is the expected error in the plasma calibration due to incoherent noise ($\sigma_y \lesssim 10^{-14}$, at integration times between 1000 and 10 000 s). We therefore require that the fluctuations in non-gravitational accelerations over a time scale τ be

$$\sigma_a \leqslant \frac{c\sigma_y}{\tau}. \tag{15}$$

Since the measurement strategy gives priority to low frequencies, we consider a time scale $\tau = 10^5$ s and obtain the conservative requirement

$$\sigma_a = 3 \times 10^{-9} \text{ cm s}^{-2}. \tag{16}$$

This value is obtained by extrapolating to a longer time scale the expected value of σ_y at 10^4 s. Although it is likely that σ_y will be slightly larger at long integration times, a precise estimate is very difficult at the moment. In any case the final stability at long integration times will depend crucially on the data processing. Particular attention should be given to the removal of low-frequency orbital and tropospheric contributions.

6.1. Direct solar radiation pressure

At a distance $D = 8$ AU from the Earth, near conjunction, the solar radiation pressure is determined almost entirely by the antenna of area $A = 1.2 \times 10^5$ cm^2, and produces an acceleration along the line of sight [40]

$$a_r = (\alpha + 2\epsilon)\frac{\Phi A \cos\delta}{cMD^2} = 1.6 \times 10^{-8}(\alpha + 2\epsilon) \text{ cm s}^{-2}, \tag{17}$$

where $M = 5600$ kg is the total mass of the spacecraft and $\Phi = 1.4 \times 10^6$ erg cm^{-2} s^{-1} is the solar constant; α and ϵ are, respectively, the absorption and reflection coefficients of the

dish. None of the time-varying quantities in equation (17) can drift so much that condition (16) is violated. Indeed, the variations of the solar constant and thermo-optical coefficients of the antenna are surely much smaller than 10% over the duration of the experiment. Also the change in the Sun's aspect angle δ does not produce significant effects; the acceleration a_r varies as $\delta^2/2$ near conjunction and therefore $\sigma_a \simeq 1.5 \times 10^{-4} a_r$ for the geometry of Cassini conjunctions, over a time scale of ten days. It is worth pointing out that the large distance from the Sun makes the spacecraft, as indeed the experiment, largely immune to the effects of solar radiation.

6.2. Fluctuations in the solar wind

The acceleration caused by the solar wind has the same expression (17), with $(\alpha + 2\epsilon)\Phi/c$ replaced by $m_p V^2 n$, where m_p is the proton mass, $n \approx 5$ cm^{-3} is the proton density at 1 AU and $V \approx 400$ km s^{-1} is the speed of the wind. Because the density can change by as much as 100%, this acceleration is totally unpredictable, but is about 10^{-4} times smaller than the direct solar radiation pressure, and therefore completely negligible.

6.3. Emitted radio power

The recoil due to the emitted beamed radio power P produces an acceleration $a = P/(Mc)$ of the spacecraft away from the Earth. For a total radiated power of 27 W (simultaneously at X and Ka bands) the resulting acceleration is 3×10^{-9} cm s^{-2}, comparable to the limit (16). In order to meet the scientific requirements of the experiment, the radiated power will be kept constant in time, independent of the coverage from the ground stations. It seems, however, that one could still tolerate a few power cycles of the onboard transmitter, as in case of failures or operational emergencies.

6.4. Anisotropic thermal radiation of the spacecraft

Any difference in temperature between parts of the spacecraft produces a force and a torque. The torque is counteracted by the attitude control system, through a set of reaction wheels. The exact evaluation of this force would require an accurate thermal model of the spacecraft. Thermal anisotropies are due to the complicated distribution of the thermal inputs. The main thermal emission is due to the spacecraft radioisotope generators (RTG), which provide about 20 kW of thermal power. This quantity is actually two orders of magnitude larger than the solar received power at 8 AU. Cassini exploits three cylindrical RTG, mounted asymmetrically on booms around the spacecraft main engine. Most of the power will be radiated from each RTG in a symmetrical pattern, but the residual anisotropy could still produce a significant effect. What matters here is that the emission pattern is constant in time, since the RTGs have a fixed orientation with respect to the spacecraft and, as an accepted scientific requirement, the spacecraft will be in a stable thermal mode, with no change in the electrical loads. In this situation, the RTGs' thermal control system, based on actively controlled louvres, will not produce changes in the radiated power. Let us assume as a realistic case that 10% of the thermal power P_{RTG} is emitted along a constant but unknown direction with respect to the spacecraft. The only changes in the radial acceleration are therefore due to the tiny attitude motions required to keep the high-gain antenna (HGA) constantly pointed toward the Earth. The attitude control system will provide a pointing accuracy of better than $\Delta\beta = 0.1^\circ$, so that the resulting change in acceleration will amount to $a \approx 0.1 P_{RTG}\, \Delta\beta/(Mc) \simeq 5 \times 10^{-10}$ cm s^{-2}, i.e. below the threshold (16).

6.5. Attitude changes

As the centre of phase of the HGA does not coincide with the centre of mass of the spacecraft, attitude control motions give rise to a Doppler shift in the received ground signal. During all cruise radio science experiments the 4 m paraboloid is constantly pointed toward the Earth by means of reaction wheels, which provide three-axis stabilization of the spacecraft. A spacecraft rotation with angular velocity $\boldsymbol{\Omega}$ (almost orthogonal to the Earth-pointing unit vector $\boldsymbol{E}$) produces a two-way relative frequency shift

$$y(t) = \frac{2}{c}(\boldsymbol{\Omega} \times \boldsymbol{r}) \cdot \boldsymbol{E} \approx \frac{2\Omega d}{c}, \tag{18}$$

$\boldsymbol{r}$ being the position of the phase centre in the spacecraft frame and d its distance from the Earth–centre-of-mass line. The antenna optical axis is assumed to be parallel to the spacecraft z-axis.

Two effects are relevant: spacecraft rotations required for Earth-keeping and roll motions about the spacecraft z-axis. The attitude control system provides Earth pointing with an accuracy of 0.1°. Over a time scale of 10^5 s this corresponds to an angular velocity of about 2×10^{-8} rad s^{-1}, with a negligible contribution to the Doppler shift.

For a circularly polarized antenna, rotations about the spacecraft z-axis also produce a Doppler shift of the carrier frequency ν, of magnitude $\Omega_z/(2\pi\nu)$, independent of the position of the centre of phase. This requires a knowledge or control of the rotation along the z-axis to a level of $\sigma_\Omega < 7 \times 10^{-4}$ rad s^{-1} at Ka band. This level of accuracy is easily met.

Although thrusters will not be used during the experiment, the effect of thruster leakage has to be assessed. Although this is largely unpredictable, a previous study of this effect [41], based on data from various space missions, models the resulting stochastic fluctuations of y with a white frequency spectrum of level $S_y \approx 2 \times 10^{-32}$ Hz^{-1} in a bandwidth between 10^{-4} and 10^{-2} Hz. This is equivalent to a stochastic acceleration spectrum proportional to f^2 in the same band. The relative frequency shifts in a 10^{-4} Hz bandwidth should therefore amount to about 1.4×10^{-18}, well below the limit of 10^{-14} expected from the plasma calibration system.

7. Conclusions

Two major space projects are expected to improve the accuracy in the γ parameter in the near future. Gravity Probe-B, a relativity gyroscope experiment, is expected to improve the accuracy in γ to 6×10^{-5} [42]. The European Space Agency GAIA project is in an advanced state of planning; it consists of an astrometric interferometer at the 10 microarcsec accuracy level, to cover 15×10^6 objects in the whole celestial sphere. This accuracy will require taking into account the gravitational deflection for all stars; observations will have to be performed within a fully relativistic framework [43]. The achievable accuracy in γ requires an assessment of the global data analysis over the whole celestial sphere. It has been claimed that accuracies between 10^{-6} and 10^{-7} are possible [44]. A similar, but much less sensitive measurement has already been performed, based on observations from the ESA Hipparcos satellite [45]. In addition, the proposed ESA mission for a Mercury orbiter will provide another excellent opportunity for testing general relativity, including a measurement of γ with a precision of 10^{-5} [46]. A small Mercury relativity satellite would give comparable accuracies [47].

Several other concepts have been put forward to improve the accuracy in the γ parameter up to a cosmologically significant level. Optical interferometers on the ground, if used for two sources near the Sun, would produce outstanding accuracies [48]. None of these projects, however, has really been started yet.

A critical, and uncertain, point of the Doppler experiments is the time scale of the signal, considerably longer than the duration of a tracking pass. So far Doppler measurements have been analysed pass by pass, often fitting away in each passage the relevant components of lowest frequency, mainly determined by the orbital and tropospheric effects. We have used for the assessment of the accuracy the target value of the Allan deviation $\sigma_y(\tau) = 10^{-14}$ at $\tau = 1000$–$10\,000$ s integration time; it is difficult to know at present the accuracy at the much longer time scale of interest. For a power-law error spectrum $S_y(f) \propto f^{-p}$, the Allan deviation $\sigma_y(\tau)$ is proportional to $\tau^{(p-1)/2}$. Past experiments with Ulysses and other spacecraft have shown that, for $f < 10^{-4}$ Hz, the spectral index is in the range $0.5 < p < 1.5$. In the most pessimistic case ($p = 1.5$) one may expect an increase of the Allan deviation by a factor smaller than 2 over the decade 10^4–10^5 s. Such an increase would not significantly affect our conclusions.

In this work we did not spot any substantial obstacle that would prevent approaching a theoretical accuracy in γ of $\sigma_\gamma \simeq 10^{-5}$. This remarkable precision can be achieved by exploiting the unique engineering set-up of the onboard and ground radio system, which allows a virtually complete elimination of the plasma. By using a multi-frequency scheme, the noise level due to the solar corona is decreased by up to three orders of magnitude when the beam is within 2–3$R_\odot$. It is worth pointing out that a Ka-band link by itself, without the use of additional frequencies, would also provide significant improvement over previous measurements of γ. A preliminary simulation using a simplified coronal model has shown that accuracies of the order of 5–10 $\times$ 10^{-5} are indeed achievable [27]. Even the backup combination (figure 3(*b*)) can be used to provide a less accurate plasma calibration, which may turn out to be important in order to incorporate in the analysis the data collected at ground stations not equipped for Ka-band transmission. Cassini's experiments, with all their wealth of data, will also be very useful to investigate the dynamical structure of the corona.

Acknowledgments

The research described in this paper was performed in part while two of the authors (GG and LI) held an NRC-NASA Resident Research Associateship at the Jet Propulsion Laboratory, California Institute of Technology, under a contract with the National Aeronautics and Space Administration. BB and LI have been supported in part by the Agenzia Spaziale Italiana.

References

[1] Will C M 1993 *Theory and Experiment in Gravitational Physics* (Cambridge: Cambridge University Press)
[2] Nordtvedt K 1995 *Icarus* **114** 51
[3] Brans C and Dicke R H 1961 *Phys. Rev.* **124** 925
[4] Damour T and Nordtvedt K 1993 *Phys. Rev. Lett.* **70** 2217
[5] Damour T and Nordtvedt K 1993 *Phys. Rev.* D **48** 3436
[6] Bertotti B, Brill D and Krotkov R 1962 Experiments on gravitation *Gravitation: an Introduction to Current Research* ed L Witten (New York: Wiley)
[7] Fomalont E B and Sramek R A 1977 *Commun. Astrophys.* **7** 19
[8] Robertson D S, Carter W E and Dillinger W H 1991 *Nature* **349** 768
[9] Lebach D E, Corey B E, Shapiro I I, Ratner M I, Webber J C, Rogers A E E, Davis J L and Herring T A 1995 *Phys. Rev. Lett.* **75** 1439
[10] Eubanks T M *et al* 1997 *Advances in Solar System Tests of Gravity* paper presented at the APS Spring Meeting
[11] Shapiro I I 1964 *Phys. Rev. Lett.* **13** 789
[12] Reasenberg R D, Shapiro I I, MacNeil P E, Goldstein R B, Breidenthal J C, Brenkle J P, Cain D L, Kaufman T M, Komarek T A and Zygielbaum A I 1979 *Astrophys. J.* **234** L219
[13] Krisher T P, Anderson J D and Taylor A H 1991 *Astrophys. J.* **373** 665

[14] Anderson J D, Esposito P B, Martin W, Thornton C L and Muhleman D O 1975 *Astrophys. J.* **200** 221
[15] Shapiro I I 1964 *Lincoln Laboratory (MIT) Technical Report* p 368
[16] Bertotti B and Giampieri G 1992 *Class. Quantum Grav.* **9** 777
[17] Kinman P W 1992 *IEEE Trans. Microwave Theory Technol.* **40** 1199
[18] Campbell J K and Anderson J D 1989 *Astron. J.* **97** 1485
[19] Schubert G, Limonadi D, Anderson J D, Campbell J K and Giampieri G 1994 *Icarus* **111** 433
[20] Anderson J D, Sjogren W L and Schubert G 1996 *Science* **272** 709
[21] Woo R 1975 *Astrophys. J.* **201** 238
[22] Woo R, Armstrong J W, Sheeley N R, Howard R A, Koomen M J, Michels D J and Schwenn R 1985 *J. Geophys. Res.* **90** 154
[23] Estabrook F B and Wahlquist H D 1975 *Gen. Rel. Grav.* **6** 439
[24] Bertotti B, Ambrosini R, Asmar S W, Brenkle J P, Comoretto G, Giampieri G, Iess L, Messeri A and Wahlquist H D 1992 *Astron. Astrophys. Suppl.* **92** 431
[25] Anderson J D, Armstrong J W and Lau E L 1993 *Astrophys. J.* **408** 287
[26] Bertotti B, Ambrosini R, Armstrong J W, Asmar S W, Comoretto G, Giampieri G, Iess L, Messeri A, Vecchio A and Wahlquist H D 1995 *Astron. Astrophys.* **296** 13
[27] Giampieri G 1996 Relativity experiments in the solar system *Proc. XI Italian Conf. on General Relativity and Gravitational Physics* ed M Carfora *et al* (Singapore: World Scientific)
[28] Bertotti B, Comoretto G and Iess L 1993 *Astron. Astrophys.* **269** 608
[29] Vessot R F C and Levine M W 1979 *Gen. Rel. Grav.* **10** 181
[30] Bertotti B and Giampieri G 1998 *Solar Phys.* **178** 85
[31] Bertotti B 1998 *Gen. Rel. Grav.* **30** 209
[32] Coles W A 1978 *Space Sci. Rev.* **21** 411
[33] Armstrong J W and Woo R 1980 *Jet Propulsion Laboratory Internal Report* IOM 3331-80-070
[34] Deep Space Network/Flight Project Interface Design Handbook 1992 *JPL/DSN Document* **810–5** Review D, section TCI-40, p 10
[35] Woo R 1980 *Astrophys. J.* **219** 727
[36] Shimabukuro F I 1995 The Solar spectrum above 1 mm *The Solar Output and its Variations* ed O R White (Boulder, CO: Associated University Press)
[37] Ha T T 1990 *Digital Satellite Communications* (New York: McGraw-Hill)
[38] Morabito D 1998 Private communication
[39] Anderson J D, Laing P A, Lau E L, Liu A S, Nieto M M and Turyshev S G 1998 *Phys. Rev. Lett.* **81** 2858 (Anderson J D, Laing P A, Lau E L, Liu A S, Nieto M M and Turyshev S G 1998 *Preprint* gr-qc/9808081)
[40] Milani A, Nobili A M and Farinella P 1987 *Non-gravitational Perturbations and Satellite Geodesy* (Bristol: Hilger)
[41] Riley A L *et al* 1990 Cassini Ka-band precision Doppler and enhanced telecommunications system study *NASA-JPL and Agenzia Spaziale Italiana Report*
[42] Fitch V L *et al* 1995 *Review of Gravity Probe-B* (Washington, DC: National Academy)
[43] de Felice F, Lattanzi M G, Vecchiato A. and Bernacca P L 1998 *Astron. Astrophys.* **332** 1133
[44] Perryman M A C, Lindegreen L and Turon C 1997 The scientific goals of the Gaia mission *Proc. ESA Symp. Hypparcos* ed M A C Perryman and F van Leeuwen, ESA SP-402
[45] Froeschlé M, Mignard F and Arenou F 1997 Determination of the PPN parameter γ with the Hipparcos data *Proc. ESA Symp. Hypparcos* ed M A C Perryman and F van Leeuwen, ESA SP-402
[46] Racca G D *et al* 1997 *Mercury Cornerstone: Interim Report* ESA/PF/1462.97/GR
[47] Bender P L, Ashby N, Vincent M A and Wahr J M 1989 *Adv. Space Res.* **9** 113
[48] Shao M 1995 *Astrophys. Space Sci.* **223** 119